

DESIGN AND ANALYSIS OF WIND TURBINE SYSTEMS WITH OPEN-CIRCUIT FAULT-TOLERANT CONTROL FOR OUTER SWITCHES OF THREE-LEVEL RECTIFIERS

¹POTHKANURI PRANAVI, ²SINGAM SRIDHAR

¹M.Tech, BALAJI INSTITUTE OF TECHNOLOGY & SCIENCE

²Assistant Professor, BALAJI INSTITUTE OF TECHNOLOGY & SCIENCE

ABSTRACT-A three-level converter is used as the power converters of wind turbine systems because of their advantages such as low-current total harmonic distortion, high efficiency, and low collector-emitter voltage. Interior permanent magnet synchronous generators (IPMSGs) have been chosen as the generator in wind turbine systems owing to their advantages of size and efficiency. In wind turbine systems consisting of the three-level converter and the IPMSG, fault-tolerant controls for an open-circuit fault of switches should be implemented to improve reliability. This paper focuses on the open-circuit fault of outer switches (S_{x1} and S_{x4}) in three level rectifiers (both neutral-point clamped and T-type) that are connected to the IPMSG. In addition, the effects of S_{x1} and S_{x4} open-circuit faults are analyzed, and based on this analysis, a tolerant control is proposed. The proposed tolerant control maintains normal operation with sinusoidal currents under the open-circuit fault of outer switches by adding a compensation value to the reference voltages. The effectiveness and performance of the proposed tolerant control are verified by simulation and experiment

I. INTRODUCTION

The power capacity of a wind turbine system has been increasing consistently, leading to the development of generators with large power capacity [1]–[3]. There are many types of generators. Permanent magnet synchronous generators (PMSGs) have high efficiency and high reliability compared with induction generators. This is because external excitation is not required and there are no copper losses in the rotor circuits. Moreover, because of the smaller size of the PMSG, the weight of the wind turbine is reduced [4].

Among various PMSGs, interior PMSGs (IPMSGs) are especially advantageous from the standpoints of efficiency and power generation owing to the use of the reluctance torque [4]–[7]. Generators requiring high voltage need to use multilevel converter topologies to reduce the collector-emitter voltage per switch. Among multilevel topologies, three-level topologies such as the three-level neutral-point clamped (3L-NPC) and T-type topologies are applied in wind turbine systems with a wide power

range. The three-level topology can easily be expanded from a two-level topology and is also easier to control compared with other multilevel topologies.

Furthermore, the three-level topology guarantees high efficiency and low-current total harmonic distortion (THD) in comparison with the two level topology [8]–[11]. The 3L-NPC topology is vulnerable to switch faults because many switches are used. Switch fault detection and tolerant control methods for switch faults should be implemented to improve the reliability of wind turbine systems. Switch faults are divided into a short-circuit fault and an open-circuit fault [12]. The short-circuit fault normally leads to a breakdown of the entire system; therefore, fault detection and tolerant control methods for the short-circuit fault require additional circuits. A back-to back converter using the 3L-NPC topology is shown in Fig. 1.

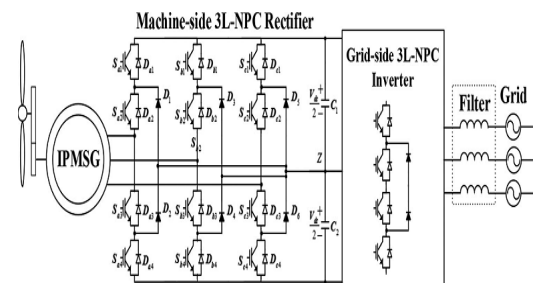


Fig. 1. Back-to-back converter using the 3L-NPC topology in wind turbine systems.

This consists of the machine-side 3L-NPC rectifier, the dc-link, and the grid-side 3L-NPC inverter. Depending on the operating conditions, tolerant controls can be applied for the rectifier or the inverter because the current paths of the rectifier and the inverter are different [9], [13]–[15]. In addition, the different structure of the three-level topologies should be considered in the tolerant controls [9], [13]. In the 3L-NPC inverter, the open-circuit fault of the inner switch causes the outer switch connected it to be infeasible; therefore, changing only the switching method does not become a solution for the open-circuit fault, and the additional devices such as fuses and switches should be added for achieving the

tolerant operation under the open-circuit fault of the inner switch [16]–[18].

However, the open-circuit fault of the outer switch can be handled by changed the switching method in limited range [19]. In [19], the tolerant control method limits the output voltage range by half. In addition, the reactive current is injected to eliminate current distortion caused by the open-circuit fault of the outer switch [22].

when rectifiers operate at a unique pf [4]–[7]. In such a case, an open-circuit fault of the outer switches (S_{x1} and S_{x4}) causes current distortion and torque fluctuation, which can lead to vibration of the wind turbine. In this paper, the reason for the current distortion caused by the outer switches (S_{x1} and S_{x4}) is analyzed, and then, on the basis of this analysis, a tolerant control for S_{x1} and S_{x4} open-circuit faults is proposed.

III. OPEN-CIRCUIT FAULT ANALYSIS OF OUTER SWITCHES

There are three switching states (P, N, and O) in the 3L-NPC rectifier [9]. Six current paths can be generated depending on the current direction and the switching state, and these are shown in Fig. 2 [23]. Fig. 3 shows the input current generation process of a rectifier with unity pf.

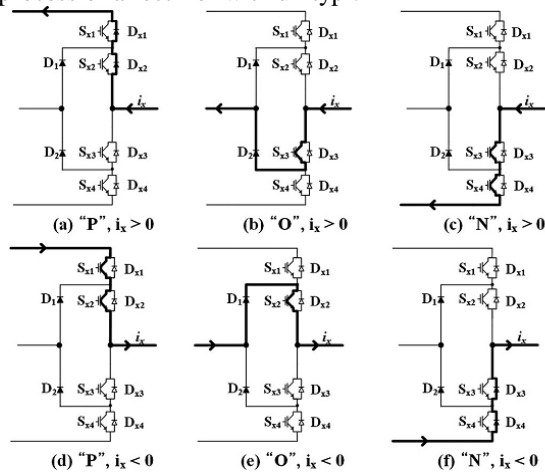
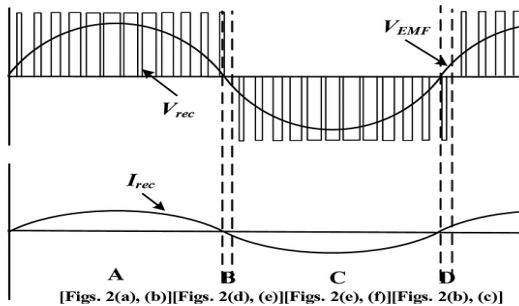


Fig. 2. Current paths depending on the current direction and the switching state.



[Figs. 2(a), (b)] [Figs. 2(d), (e)] [Figs. 2(e), (f)] [Figs. 2(b), (c)]

Fig. 3. Rectifier operation at unity pf.

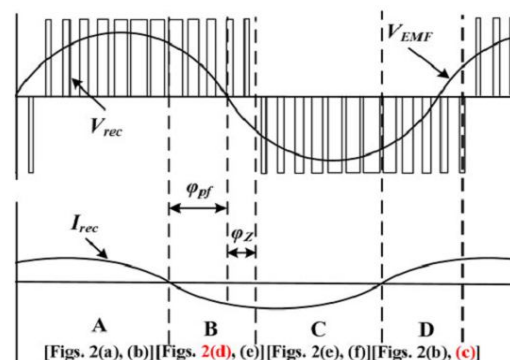
TABLE I
CURRENT PATH COMPOSITION DEPENDING ON THE PART OF FIG. 3

Part	V_{rec}	I_{rec}	Current path
A	Positive	Positive	(a) P switching state, (b) O switching state (valid)
B	Positive	Negative	(d) P switching state (valid), (e) O switching state
C	Negative	Negative	(e) O switching state (valid), (f) N switching state
D	Negative	Positive	(b) O switching state, (c) N switching state (valid)

The phase difference between V_{EMF} and V_{rec} , which causes the current flow, is controlled to match the phase of I_{rec} up with the phase of the corresponding V_{EMF} . One period of I_{rec} can be divided into four parts depending on the polarity of I_{rec} and V_{rec} . The generated current paths are different depending on the part, and these are summarized in Table I. In parts A and C, the O switching state causes the input current flow; therefore, this is called the valid switching state. The current continuously flows through two diodes if the switching state is changed to P or N switching state in which no current flows through the switches.

In parts B and D, the P and N switching states are the valid switching state where the current flows through the switches. When the rectifier operates with unity pf, parts A and C are large, and parts B and D are small.

In this paper, the other case (Case II), which is the reactive current injection for IPMSG, is also considered. Fig. 4 shows that the input current generation process of the rectifier for Cases I and II. There are two phase differences: the phase difference (ϕ_Z) between V_{EMF} and V_{rec} explained in [22], and the phase difference (ϕ_{pf}) between I_{rec} and V_{EMF} caused by the pf. In Fig. 4, part B (or part D) consists of ϕ_Z and ϕ_{pf} , and their lengths increase. This means that the current can be more distorted by the open-circuit fault of the outer switches compared to when ϕ_Z alone is considered



[Figs. 2(a), (b)] [Figs. 2(d), (e)] [Figs. 2(e), (f)] [Figs. 2(b), (c)]
Fig. 4. Rectifier operation at any pf.

Case I can be ignored because ϕ_Z is determined depending on the operating condition of the rectifier and the PMSG. However, because ϕ_{pf} is determined by the pf, Case II should be considered when the IPMSG is employed. The current distortion caused by the open-circuit fault of the outer switches is shown in Fig. 5 for various pfs. Owing to the infeasible open-circuit fault switch, the current becomes zero during the range consisting of ϕ_Z and ϕ_{pf} . The Sx1 open-circuit fault makes the current path of Fig. 2(d) infeasible.

The current path of Fig. 2(d) belongs to part B; therefore, the Sx1 open-circuit fault causes distortion in the negative current as shown in Fig. 5(a) and (c). On the contrary, the Sx4 open-circuit fault leads to distortion in the positive current as shown in Fig. 5(b) and (d) because the current path of Fig. 2(c) related to the Sx4 open-circuit fault belongs to part D. The low pf has a large ϕ_{pf} . Therefore, the rectifier operation at a low pf leads to a large zero-current range when the open-circuit fault of the outer switch occurs. As a result, the zero-current range increases, as the pf decreases.

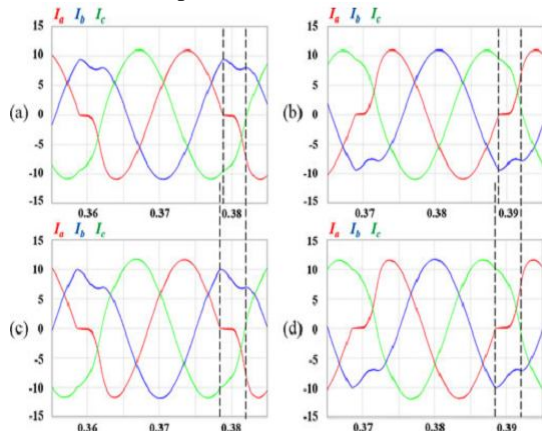


Fig. 5. Current distortion depending on the open-circuit fault and the pf: (a) 0.95pf, Sx1 open-circuit fault, (b) 0.95pf, Sx4 open-circuit fault, (c) 0.9pf, Sx1 open-circuit fault, and (d) 0.9pf, Sx4 open-circuit fault

The analysis related to the open-circuit fault of the outer switches can be applied to the T-type topology. The effects of open-circuit faults of the outer switches on the current are the same in both the NPC rectifier and the T-type rectifier [13], [22]. Therefore, the current distortion caused by open-circuit faults of the outer switches in the NPC rectifier is the same as that in the T-type rectifier.

III. TOLERANT CONTROL FOR OPEN-CIRCUIT FAULT OF OUTER SWITCHES

An existing tolerant control method for the open-circuit fault of the outer switches is reactive current injection [22]. This method changes the phase offset so that it corresponds with the phase of V_{rec} . This means that parts B and D are eliminated. However, this tolerant control method has the disadvantage of low-power generation efficiency of the generator because the PMSG has efficient operating condition which depends on the pf of the rectifier. The proposed tolerant control does not change the pf of the rectifier. The rectifier voltage (V_{rec}) without the current path related to the open-circuit fault switch is generated by changing the reference voltages. To explain the proposed tolerant control, the Sx1 open-circuit fault is used as an example.

A. Compensation Voltage (V_{comp}) Calculation

Three-phase reference voltages ($V_{x,ref}$, $x=a, b, c$) are expressed as

$$\begin{aligned} V_{a,ref} &= V_{mag} \cos(2\pi f_s t) \\ V_{b,ref} &= V_{mag} \cos(2\pi f_s t - 2\pi/3) \\ V_{c,ref} &= V_{mag} \cos(2\pi f_s t + 2\pi/3) \end{aligned} \quad (1)$$

Where V_{mag} is the magnitude of the reference voltages, and f_s is the fundamental frequency. The offset voltage (V_{offset}) is added to each reference voltage to expand the range of the modulation index ($M_a = \sqrt{3} \times V_{mag}/V_{dc}$). V_{offset} and the changed reference voltages ($V_{x,ref,offset}$, $x=a, b, c$) are expressed as

$$V_{offset} = -\frac{(V_{ref,max} + V_{ref,min})}{2} \quad (2)$$

$$\begin{aligned} V_{a,ref,offset} &= V_{a,ref} + V_{offset} \\ V_{b,ref,offset} &= V_{b,ref} + V_{offset} \\ V_{c,ref,offset} &= V_{c,ref} + V_{offset} \end{aligned} \quad (3)$$

Where $V_{ref,max}$ and $V_{ref,min}$ are the maximum and minimum values of $V_{a,ref}$, $V_{b,ref}$, and $V_{c,ref}$. The reference voltages of (3) are compared with the carrier signals to generate V_{rec} . When the Sx1 open-circuit fault occurs, the current path of Fig. 2(d) should be eliminated to prevent current distortion; therefore, the reference voltage should be changed to generate V_{rec} without the current path of Fig. 2(d). In the proposed tolerant control, a reference voltage of a phase containing the Sx open-circuit fault is changed to zero as shown in Fig. 6. As a result, the current path of Fig. 2(d) disappears because the O switching state is only used in part B. To make the reference voltage zero, $|V_{comp}|$ is assigned the magnitude of the reference voltage ($V_{x,ref,offset}$) containing the open-circuit fault, and V_{comp} can be expressed as

$$V_{comp} = -V_{x,ref,offset} \quad (x = a \text{ phase containing open circuited fault switch}) \quad (4)$$

The proposed tolerant control is implemented by adding V_{comp} to the reference voltages ($V_{x,ref,offset}$, $x=a, b, c$). The new reference voltages ($V_{x,ref,tolerance}$, $x=a, b, c$) of the proposed tolerant control are expressed as

$$\begin{aligned} V_{a,ref,tolerance} &= V_{a,ref,offset} + V_{comp} \\ V_{b,ref,tolerance} &= V_{b,ref,offset} + V_{comp} \\ V_{c,ref,tolerance} &= V_{c,ref,offset} + V_{comp} \end{aligned} \quad (5)$$

B. Compensation Range for Adding V_{comp}

By adding V_{comp} to each reference voltage, the use of the current path related to the open-circuit fault switch will be precluded. To achieve this perfectly, V_{comp} is added for the suitable range and position. The compensation range, which is part B or part D of Fig. 4, consists of ϕ_Z and ϕ_{pf} . ϕ_Z can be calculated with the equivalent circuit of the PMSG and the three-level rectifier [22]. ϕ_Z , which is the phase difference between V_{EMF} and V_{rec} , is expressed as

$$\phi_Z = \tan^{-1} \left(\frac{-|I_{rec}| * 2\pi f_s L}{V_{EMF} - |I_{ref}| R} \right) \quad (6)$$

where R and L are the equivalent resistance and inductance of the PMSG, and f_s is the fundamental frequency representing the angular frequency of the PMSG. ϕ_{pf} , which is the phase difference between V_{EMF} and I_{rec} , is related to the pf . ϕ_{pf} can be calculated by the pf and this is expressed as

$$\phi_{pf} = \cos^{-1}(pf) \quad (7)$$

If the d-q control theorem is used, ϕ_{pf} can be calculated as

$$\phi_{pf} = \cos^{-1} \left(\frac{I_{qe}}{\sqrt{I_{qe}^2 + I_{de}^2}} \right) \quad (8)$$

Where I_{de} indicates the d-axis current related to the flux and I_{qe} indicates the q-axis current related to the torque, and these are values in the d-q synchronous rotating frame. ϕ_Z and ϕ_{pf} , which are calculated from (6) and (8), are located near the zero-crossing point of V_{EMF} as shown in Fig. 6. Therefore, the compensation position for adding V_{comp} is defined on the basis of V_{EMF} 's angle (θ_{EMF}).

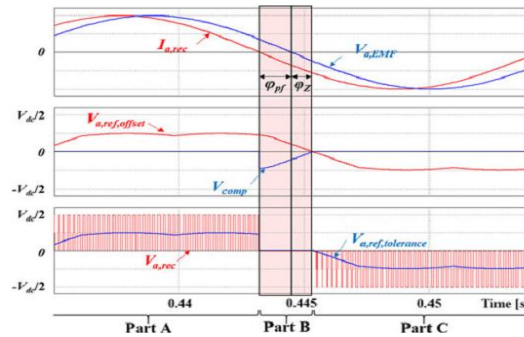


Fig. 6. Change of reference voltages in the proposed tolerant control for the S_{x1} open-circuit fault (0.95 pf).

Fig. 7 shows three-phase V_{EMF} and θ_{EMF} . θ_{EMF} is acquired from the encoder or position sensor. Six zero-crossing points are expressed for every 60° , which are matched to each open-circuit fault as shown in Fig. 7. Consequently, θ_{EMF} representing each zero-crossing point is a criterion for adding V_{comp} . For example, when the S_{a1} open-circuit fault occurs, V_{comp} should be added for the compensation range from $(0 - \phi_{pf})$ to $(0 + \phi_Z)$ which is based on 0° . By considering all open-circuit faults, Table II shows the compensation ranges for eliminating the current distortion depending on the position of the open-circuit fault

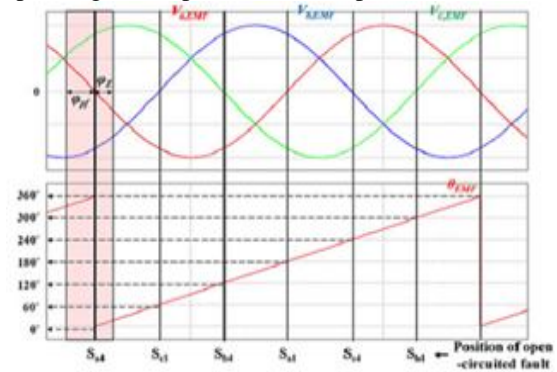


Fig. 7. Compensation position on the basis of V_{EMF} 's angle (θ_{EMF}).

Table II
compensation range depending on the position of the open-circuit fault

Position of open-circuit fault	Compensation range
S_{a1}	$(0^\circ - \varphi_{pf}) \sim (0^\circ + \varphi_Z)$
S_{c4}	$(60^\circ - \varphi_{pf}) \sim (60^\circ + \varphi_Z)$
S_{b1}	$(120^\circ - \varphi_{pf}) \sim (120^\circ + \varphi_Z)$
S_{a4}	$(180^\circ - \varphi_{pf}) \sim (180^\circ + \varphi_Z)$
S_{c1}	$(240^\circ - \varphi_{pf}) \sim (240^\circ + \varphi_Z)$
S_{b4}	$(300^\circ - \varphi_{pf}) \sim (300^\circ + \varphi_Z)$

C. Considering Neutral-Point Voltage Balance

The compensation voltage which is one of the offset voltages can cause neutral-point voltage unbalance because V_{comp} calculated from (4) is a one-sided voltage.

Fig. 8 shows the concept of proposed tolerant control considering the neutral-point voltage balance when the S_{a1} open-circuit fault occurs. In Fig. 8, V_{comp} is added for the compensation range $[(0^\circ - \varphi_{pf}) \sim (0^\circ + \varphi_Z)]$ which corresponds to the position for the S_{a1} open-circuit fault; in addition, V_{comp} is also added for the diametrically opposite compensation range $[(180^\circ - \varphi_{pf}) \sim (180^\circ + \varphi_Z)]$, which is the range for the S_{a4} open-circuit fault. The final principles of the proposed tolerant control with the neutral-point voltage balance are summarized in Table III.

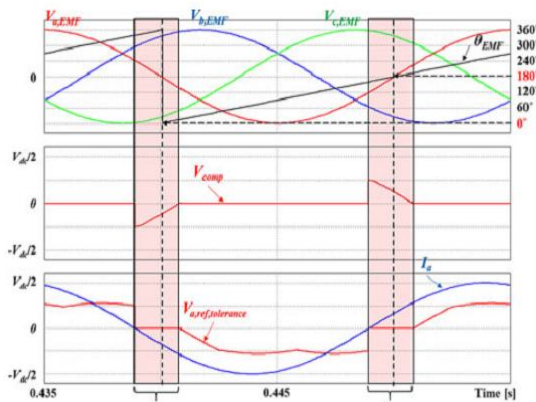


Fig. 8. Proposed tolerant control considering neutral-point voltage balance under the S_{a1} open-circuit fault
Table III

principle of the proposed tolerant control depending on the position of the open-circuit fault

Position of open-circuit fault	V_{comp}	Compensation range
S_{a1} or S_{a4}	$-V_{a,ref,offset}$	$(0^\circ - \varphi_{pf}) \sim (0^\circ + \varphi_Z)$
S_{c4} or S_{c1}	$-V_{c,ref,offset}$	$(60^\circ - \varphi_{pf}) \sim (60^\circ + \varphi_Z)$
S_{b1} or S_{b4}	$-V_{b,ref,offset}$	$(120^\circ - \varphi_{pf}) \sim (120^\circ + \varphi_Z)$
S_{a4} or S_{a1}	$-V_{a,ref,offset}$	$(180^\circ - \varphi_{pf}) \sim (180^\circ + \varphi_Z)$
S_{c1} or S_{c4}	$-V_{c,ref,offset}$	$(240^\circ - \varphi_{pf}) \sim (240^\circ + \varphi_Z)$
S_{b4} or S_{b1}	$-V_{b,ref,offset}$	$(300^\circ - \varphi_{pf}) \sim (300^\circ + \varphi_Z)$

D. Limitation of Proposed Tolerant Control

$V_{x,ref,tolerance}$ cannot exceed a limitation voltage (V_{limit}) which is restricted by the dc-link voltage (V_{dc}). Therefore, V_{comp} is limited as follows

$$V_{comp} < V_{limit} - V_{ref,max} \quad (9)$$

Where V_{limit} is $V_{dc}/2$. On the basis of (9), the applicable operation range of the proposed tolerant control is determined depending on M_a and the pf. Fig. 9 shows $V_{x,ref,tolerance}$ and V_{comp} of the proposed tolerant control depending on the pf when M_a is 0.5. In Fig. 9, V_{comp} leads to $V_{a,ref,tolerance}$ with zero value in the corresponding compensation range. Moreover, the peak value of $V_{c,ref,tolerance}$ increases owing to V_{comp} .

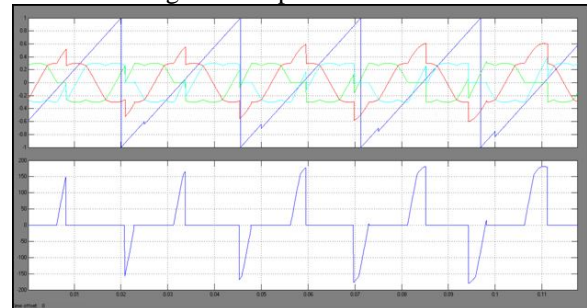


Fig. 9. $V_{x,ref,tolerance}$ ($x=a,b,c$) and V_{comp} depending on the pf when M_a is 0.5.

As the pf decreases, this peak value increases; however, it does not exceed V_{limit} . Consequently, when M_a is smaller than 0.5, V_{comp} can be added regardless of the pf because $V_{c,ref,tolerance}$ cannot exceed V_{limit} . When M_a is larger than 0.5, the applicable pf range is determined by M_a . This is because a low M_a provides a large margin for V_{comp} ; however, a large V_{comp} cannot be acceptable for high M_a . Fig. 10 shows the applicable pf range for various values of M_a . The shaded part of Fig. 10 represents the applicable operation range. The proposed tolerant control is feasible over the entire factor range when M_a is smaller than 0.5. By increasing M_a from 0.5, the applicable operation range decreases.

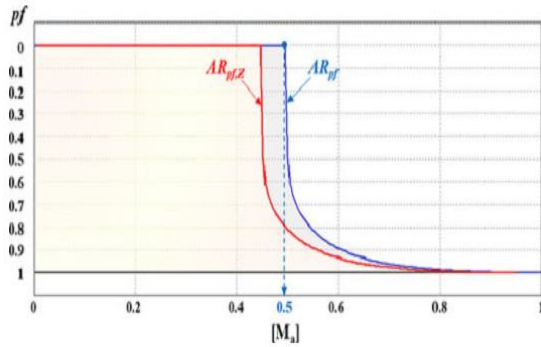
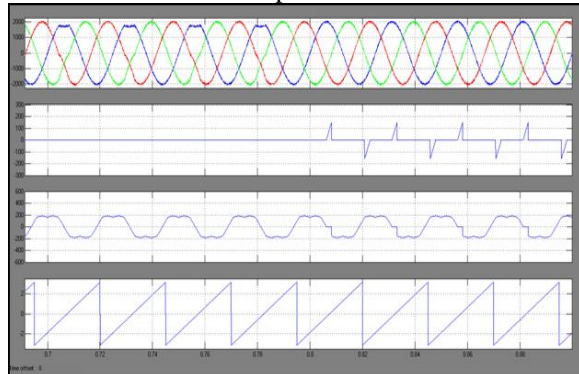


Fig. 10. Applicable pfrange of the proposed tolerant control depending on M_a .

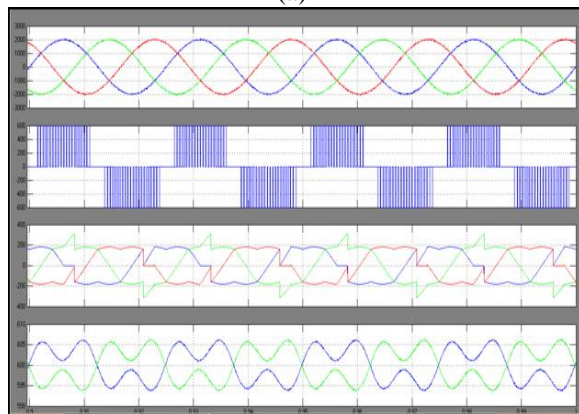
In Fig 10, the applicable operation range shown as AR_{pf} is largest when only the pf related to ϕ_{pf} is taken into account. However, a large ϕ_Z means that large portion of the compensation range is reserved for ϕ_Z , and the rest can be used to compensate ϕ_{pf} .

IV. SIMULATION RESULTS

The simulation is performed using the PSIM tool. The 3L-NPC rectifier of the back-to-back converter with 2.5-MW IPMSG is only considered in the simulation. Fig. 11 shows the simulation results of the proposed tolerant control when the Sa1 open-circuit fault occurs. The speed.



(a)



(b)

Fig. 11. Simulation results with the proposed tolerant control under the Sa1 open-circuit fault (600 rpm, $M_a = 0.35, 0.95$ pf).

Table IV
ipmsg parameters in simulation

Rated power	2.5 MW
Number of pole	8
Rated voltage (line-to-line)	760 V _{rms}
Rated current	1902 A _{rms}
Rated speed	1650 rpm
Resistance	0.4567 mΩ
q-inductance	0.0982 mH
d-inductance	0.0725 mH

As a result, the a-phase pole voltage (V_{an}) is clamped to 0 at their ranges as shown in Fig. 11(b) and the current distortion is eliminated completely.

In addition, the two dc-link capacitor voltages are balanced. The proposed tolerant control is effective for the pf transition operation of the rectifier. Fig. 12 shows the results when the proposed tolerant control is applied and the pf is changed from 0.95 to 0.9.

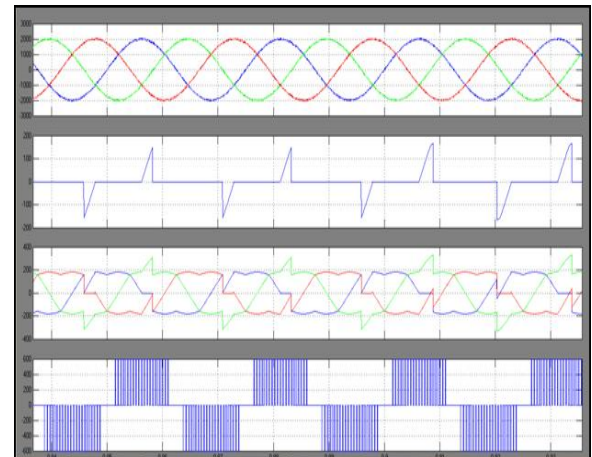


Fig. 12. Simulation results with the proposed tolerant control under the Sa1 open-circuit fault (600 rpm, $M_a = 0.35$, pf -transition from 0.95 to 0.9).

Fig. 13 shows the performance of the proposed tolerant control under the Sa1 open-circuit fault at different speed (1000 rpm) of the PMSG when M_a is 0.59. Similar to Fig. 11, the distorted currents are corrected after the proposed tolerant control is applied. However, the peak value of $V_{c,ref}$ tolerance is close to $V_{limit}(V_{dc}/2)$ at 0.95 pf, which is different from what is shown in Fig. 11. This is because M_a of Fig. 13 has a smaller.

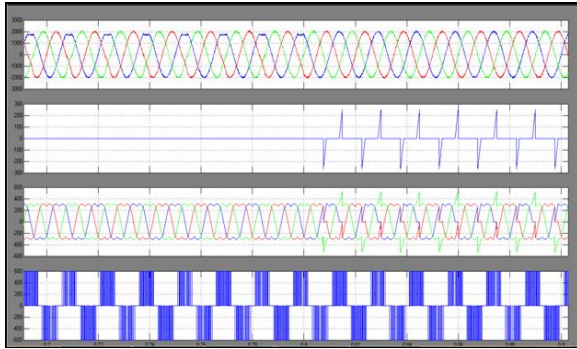


Fig. 13. Simulation results with the proposed tolerant control under the Sa1 open-circuit fault (1000 rpm, $M_a = 0.59, 0.95$ pf)

Table V shows the current THD results before and after the proposed tolerant control is applied. The current THD is increased by the Sa1 open-circuit fault; however, owing to the proposed tolerant control, the current THD is restored as good as normal state without any open-circuit fault.

VI. CONCLUSION

This paper proposes a tolerant control for the open-circuit fault of the outer switches in three-level rectifiers (both 3L-NPC and T-type topologies) used in wind turbine systems. The reason why the tolerant control for the open-circuit fault of the outer switches in three-level rectifiers is necessary is presented, together with the supporting circuit analysis. On the basis of the analysis, a tolerant control for each open-circuit fault is proposed that takes into account the neutral-point voltage balance. This control is implemented by adding a compensation voltage (V_{comp}) to the reference voltages for the corresponding compensation ranges depending on the position of the open-circuit fault. Furthermore, this control can be used in both the 3L-NPC and T-type rectifiers and guarantees normal operation without a change of the pf in the applicable operation range shown in Fig. 10 depending on the modulation index (M_a) and the pf. Although the operating range of the proposed tolerant control is subject to a limitation, considering that wind turbine systems do not always operate with the rated wind speed and that the operating pf of the rectifier with an IPMSG is not too low, the proposed tolerant control is clearly effective. The performance and effectiveness of the proposed tolerance control are proved through simulations.

REFERENCES

[1] A. Isidori, F. M. Rossi, F. Blaabjerg, and K. Ma, "Thermal loading and reliability of 10-MW multilevel wind power converter at different wind roughness classes," *IEEE Trans. Ind. Appl.*, vol. 50, no. 1, pp. 484–494, Jan./Feb. 2014.

[2] H. G. Jeong, K. B. Lee, S. Chio, and W. Choi, "Performance improvement of LCL-filter-based grid-connected inverters using PQR power transformation," *IEEE Trans. Power Electron.*, vol. 25, no. 5, pp. 1320–1330, May 2010.

[3] S. Li, T. A. Haskew, R. P. Swatloski, and W. Gathings, "Optimal and direct-current vector control of direct-driven PMSG wind turbines," *IEEE Trans. Power Electron.*, vol. 27, no. 5, pp. 2325–2337, May 2012.

[4] W. Qiao, L. Qu, and R. G. Harley, "Control of IPM synchronous generator for maximum wind power generation considering magnetic saturation," *IEEE Trans. Ind. Appl.*, vol. 45, no. 3, pp. 1095–1105, May/June 2009.

[5] S. Morimoto, H. Nakayama, M. Sanada, and Y. Takeda, "Sensorless output maximization control for variable-speed wind generation system using IPMSG," *IEEE Trans. Ind. Appl.*, vol. 41, no. 1, pp. 60–67, Jan./Feb. 2005.

[6] Y. Zhao, W. Qiao, and L. Wu, "An adaptive quasi-sliding-mode rotor position observer-based sensorless control for interior permanent magnet synchronous machines," *IEEE Trans. Power Electron.*, vol. 28, no. 12, pp. 5618–5629, Dec. 2013.

[7] P. B. Reddy, A. M. EL-Refaei, and K. K. Huh, "Effect of number of layers on performance of fractional-slot concentrated-windings interior permanent magnet machines," *IEEE Trans. Power Electron.*, vol. 30, no. 4, pp. 2205–2218, Apr. 2015.

[8] J. S. Lee and K. B. Lee, "New modulation techniques for a leakage current reduction and a neutral-point voltage balance in transformerless photovoltaic systems using a three-level inverter," *IEEE Trans. Power Electron.*, vol. 29, no. 4, pp. 1720–1732, Apr. 2014.

[9] U. M. Choi, H. G. Jeong, K. B. Lee, and F. Blaabjerg, "Method for detecting an open-switch fault in a grid-connected NPC inverter system," *IEEE Trans. Power Electron.*, vol. 27, no. 6, pp. 2726–2739, Jun. 2012.

[10] U. M. Choi, J. S. Lee, and K. B. Lee, "New modulation strategy to balance the neutral-point voltage for three-level neutral-clamped inverter systems," *IEEE Trans. Energy Convers.*, vol. 29, no. 1, pp. 91–100, Mar. 2014.